Sonication-induced Electrostatic Assembly of $FeCO_3$@Ti_3C_2 Nanocomposite for Robust Lithium Storage

Shiqi Yang,[a, b,#] *Junyi Yao,*[a, b,#] *Huimin Hu,*[a, b,#] *Youze Zeng,*[a, b] *Xue Huang,*[a, b] *Tingting Liu,*[c] *Liangmin Bu,*[a, b] *Kai Tian,*[a, b] *Yanping Lin,*[a, b] *Xiangyi Li,*[a, b] *Shuli Jiang,*[a, b] *Shaowen Zhou,*[a, b] *Wanying Li,*[a, b] *Tariq Bashir,*[a, b] *Jin-Ho Choi,*[a, b] *Lijun Gao,*[a, b, *] *and Jianqing Zhao*[a, b, *]

[a] College of Energy, Soochow Institute for Energy and Materials InnovationS (SIEMIS), Soochow University, Suzhou 215006, China.

[b] Key Laboratory of Advanced Carbon Materials and Wearable Energy Technologies of Jiangsu Province, Soochow University, Suzhou 215006, China.

[c] Suzhou University of Science and Technology & Jiangsu Key Laboratory of Environmental Science and Engineering, Suzhou 215001, China.

[#] These authors equally contributed to this work.

Corresponding Authors:

Prof. Lijun Gao, E-mail: gaolijun@suda.edu.cn

Prof. Jianqing Zhao, E-mail: jqzhao@suda.edu.cn

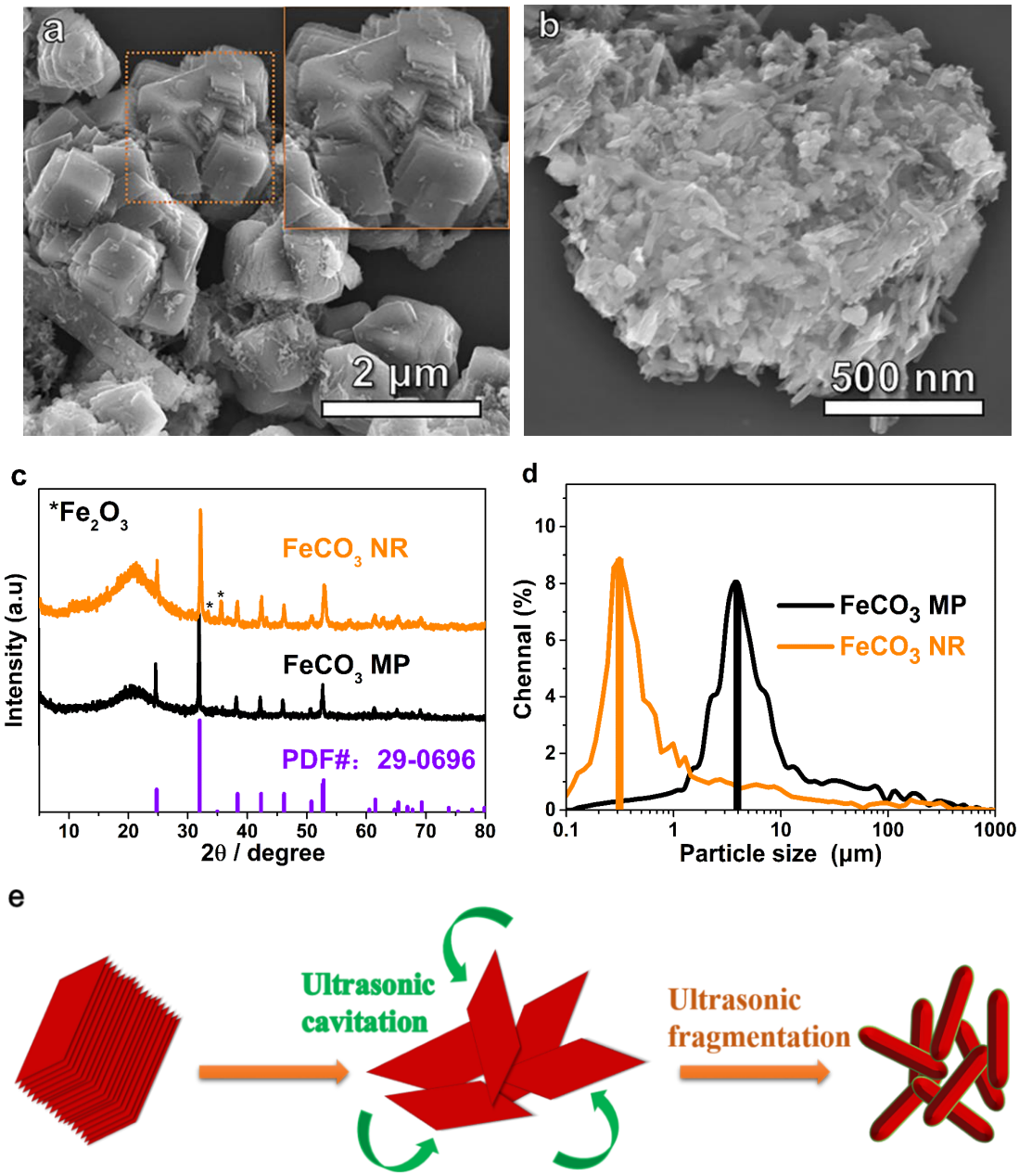

Figure S1. FESEM images of (a) $FeCO_3$ MP microparticles and (b) $FeCO_3$ NR nanorods, together with (c) XRD patterns and (d) PSD profiles of these two samples. (e) Schematics illustrating the reshaping from original $FeCO_3$ MP microparticles to $FeCO_3$ NR nanorods *via* a simple high-energy sonication treatment. The inset in (a) shows zoom-in view of $FeCO_3$ MP microparticles with the lamellar structure.

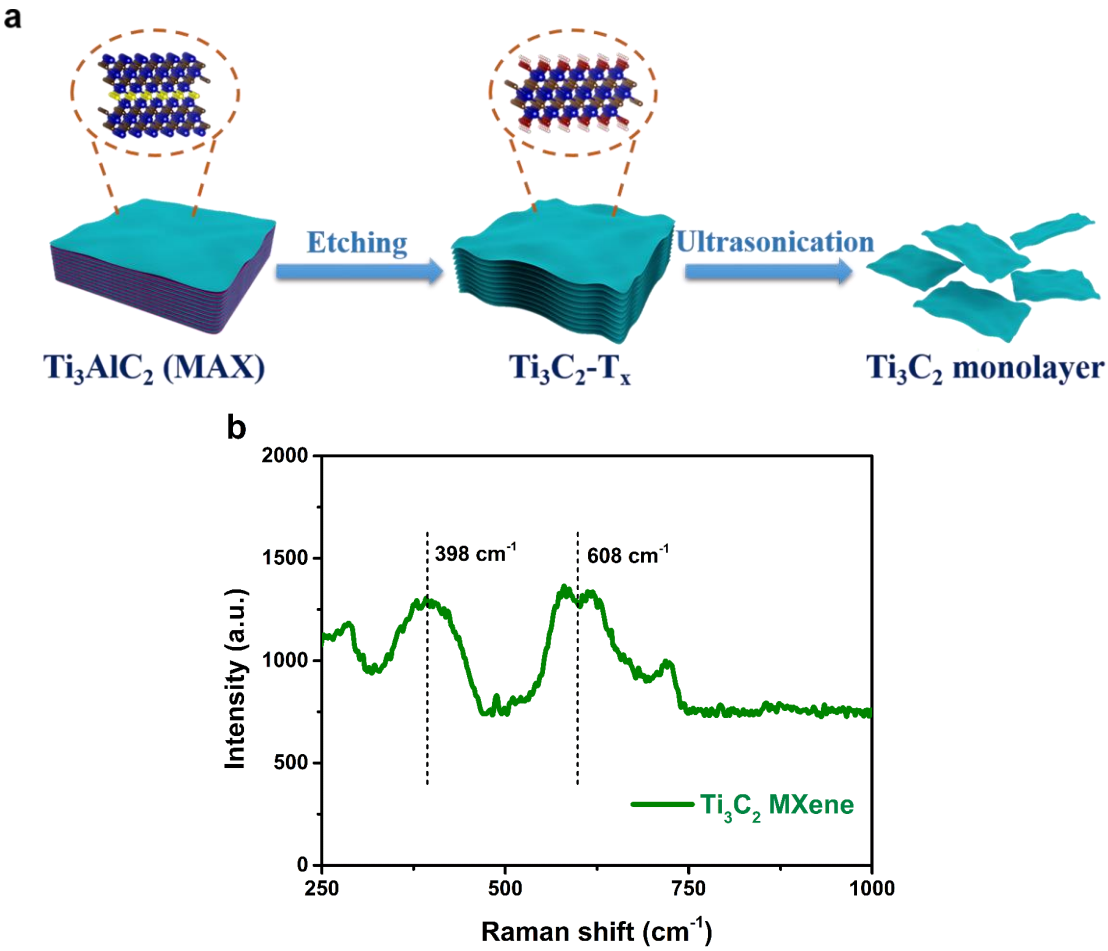

Figure S2. (a) Schematics illustrating a routine preparation of stacked and exfoliated Ti_3C_2-based MXene sheets and (b) Raman spectrum of collected Ti_3C_2 sheets, showing dominant Raman peaks at approximately 398 and 608 cm^{-1}. [S1, S2]

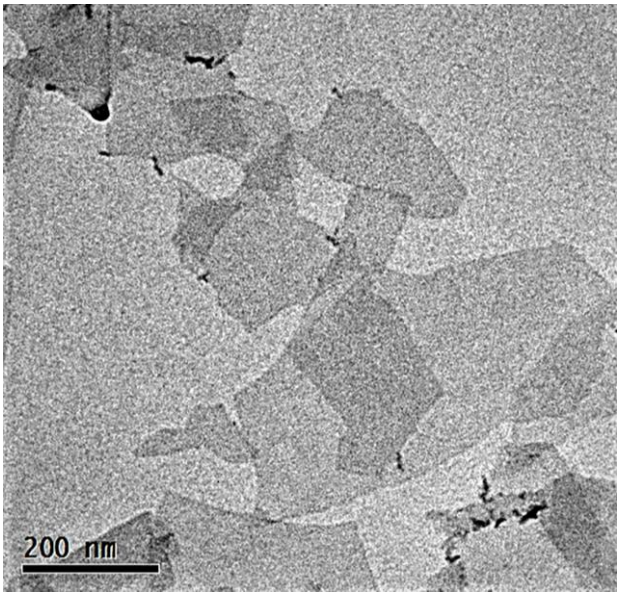

Figure S3. TEM image of highly-exfoliated Ti_3C_2 monolayers.

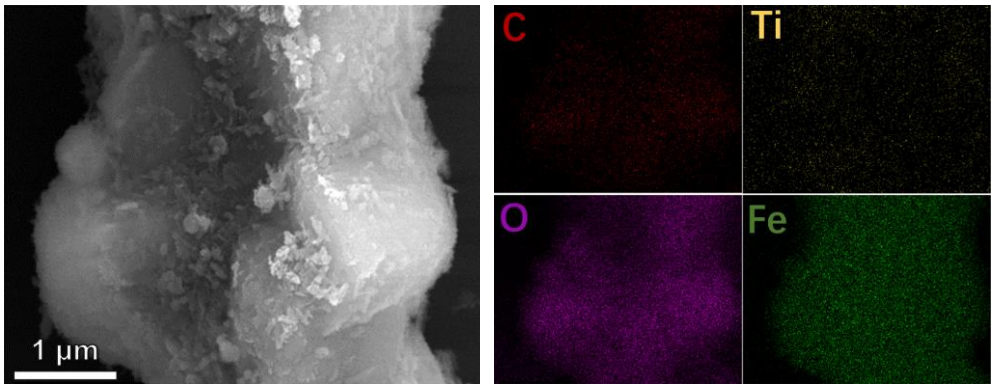

Figure S4. FESEM image of the $FeCO_3$ NR@Ti_3C_2 sample, together with corresponding EDS mappings of C, Ti, O and Fe elements.

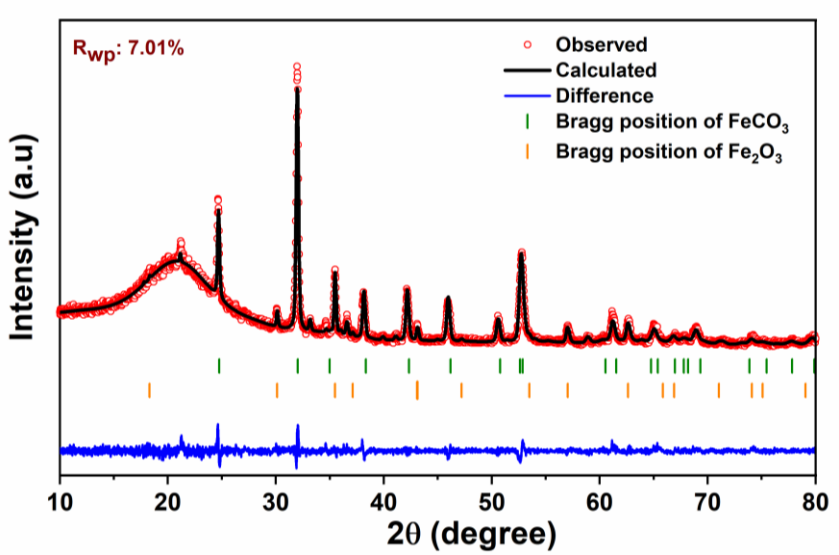

Figure S5. XRD pattern of the $FeCO_3$ NR@Ti_3C_2 sample coupled with the quantitative refinement analysis, revealing the Fe_2O_3 content of approximately 8.5 wt.% within the integrated $FeCO_3$/Fe_2O_3 composite material.

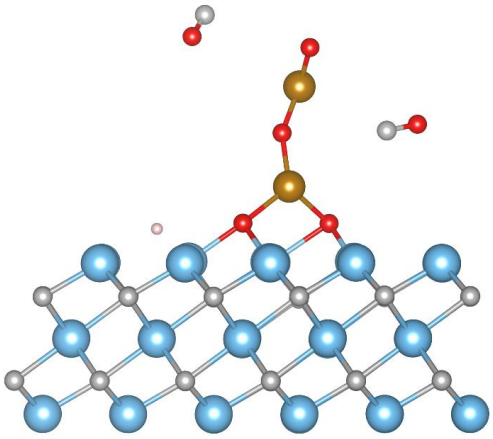

Figure S6. The optimized structure of $FeCO_3/Ti_3C_2$ through DFT calculations, revealing the structure dispersion of $FeCO_3$ after the structural optimization, when it was connected with the Ti_3C_2 substrate through the hydroxyl group, which is predominant at the surface of Ti_3C_2 component. The blue, grey, brown, red and pink circles represent Ti, C, Fe, O and H atoms, respectively.

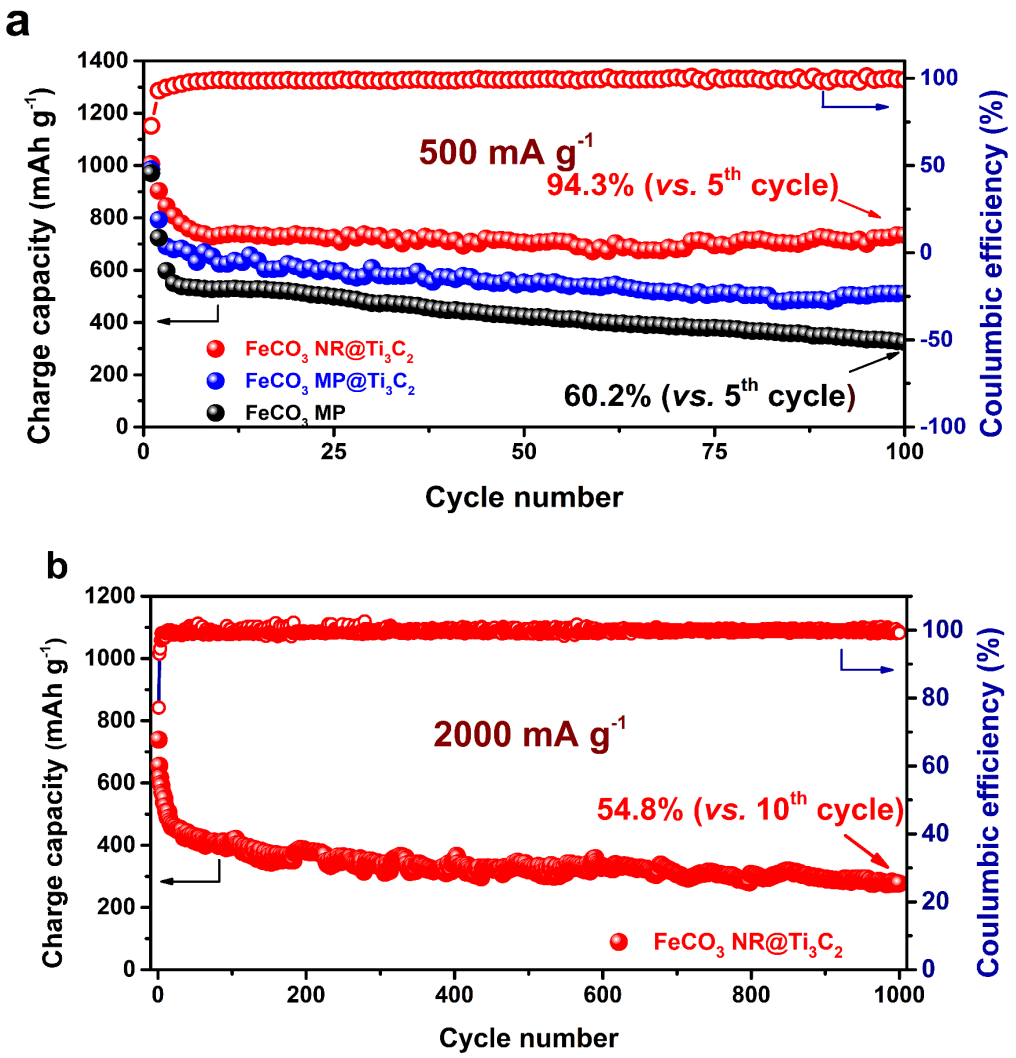

Figure S7. Cycling performance of the $FeCO_3$ NR@Ti_3C_2 anode in comparison with $FeCO_3$ MP and $FeCO_3$ MP@Ti_3C_2 in a voltage range of 0.01-3.0 V *vs.* Li^+/Li: (a) Cycled at 500 mA g^{-1} for 100 cycles and (b) Cycled at 2000 mA g^{-1} for 1000 cycles.

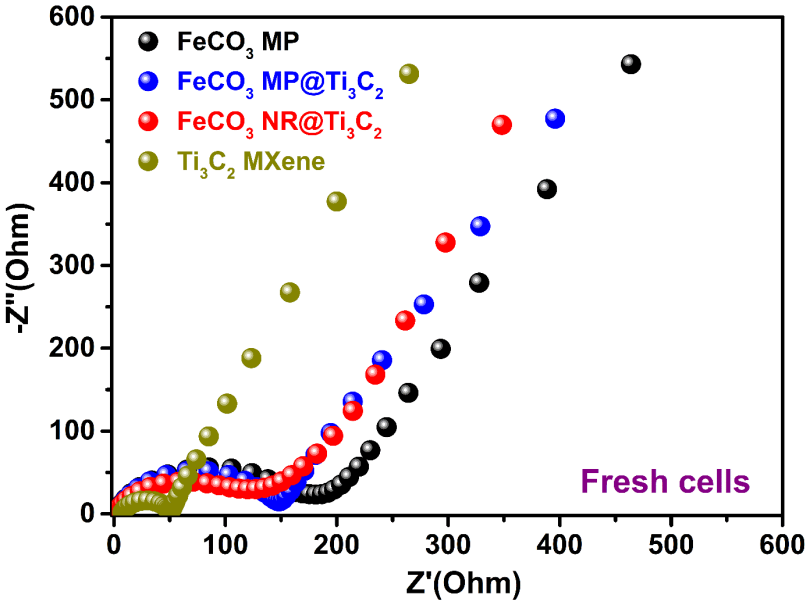

Figure S8. EIS spectra recorded on fresh cells of pure Ti_3C_2, $FeCO_3$ MP, $FeCO_3$ MP@Ti_3C_2 and $FeCO_3$ NR@Ti_3C_2 anode materials before the cell cycling.

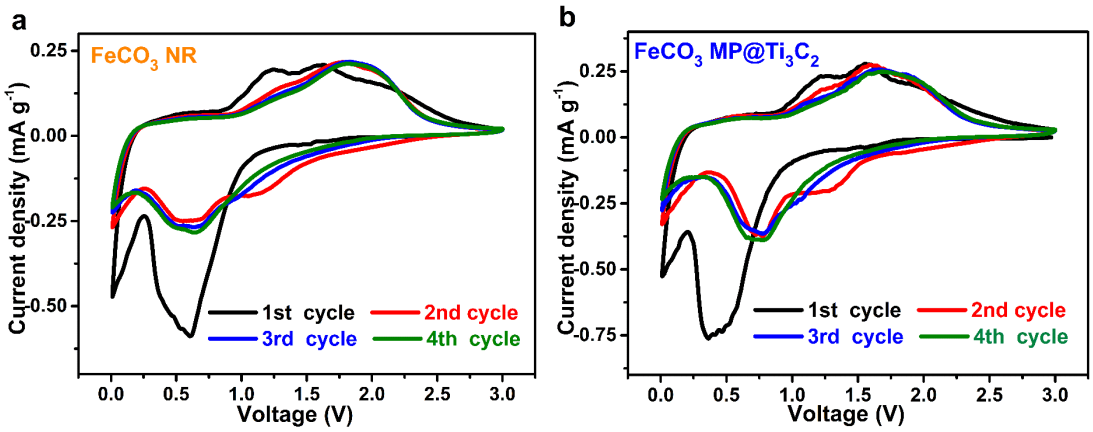

Figure S9. CV profiles of (a) $FeCO_3$ NR and (b) $FeCO_3$ MP@Ti_3C_2 anodes in the first four cycles recorded at a scanning rate of 0.1 mV s^{-1}, respectively.

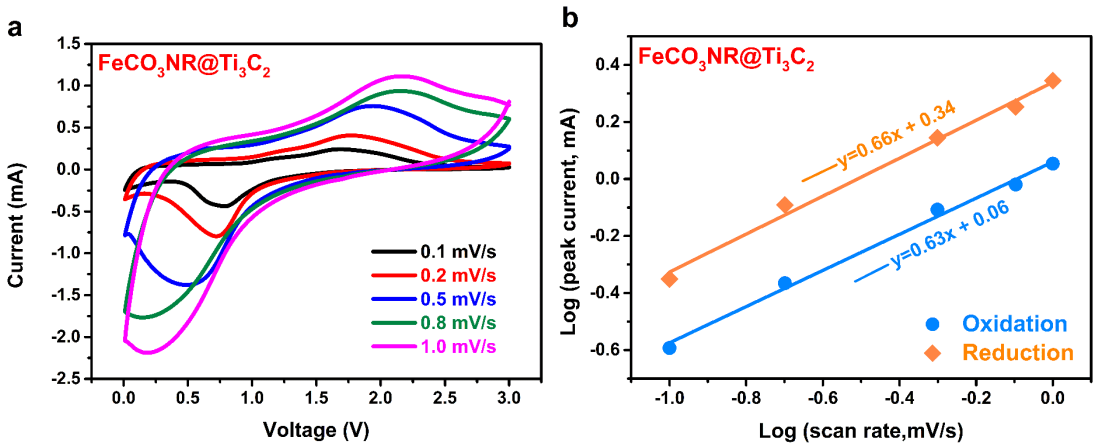

Figure S10. (a) CV curves in the 3rd cycle of $FeCO_3$ NR@Ti_3C_2 anode recorded at gradually-increased scanning rates from 0.1 to 1.0 mV s^{-1} and (b) Corresponding the logarithm of peak current (log[i_p]) and the logarithm of scanning rate (log[v]) with preferable linear fittings for both oxidation and reduction reactions.

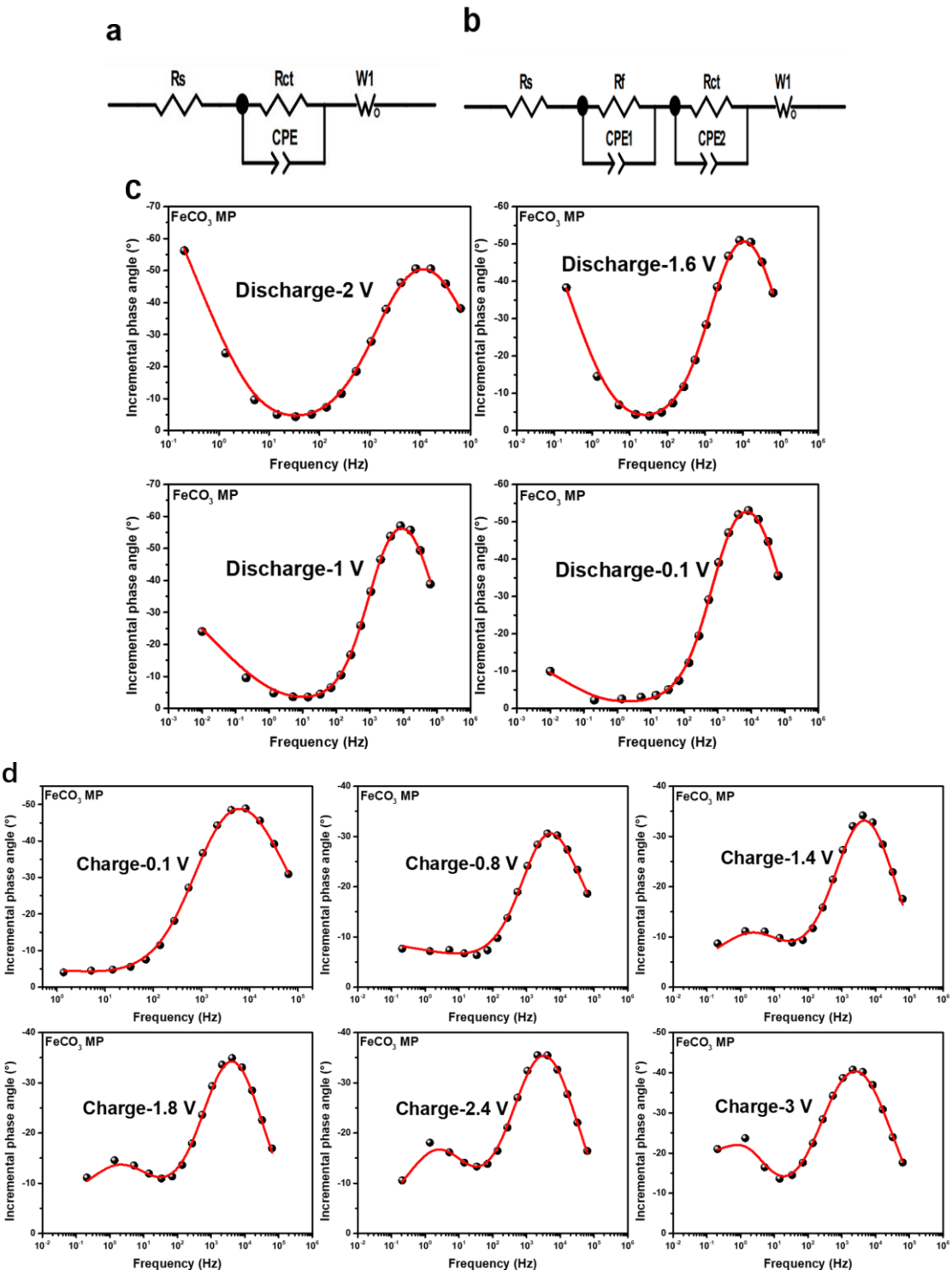
a
Rs
Rct
W1
CPE
b
Rs
Rf
Rct
W1
CPE1
CPE2
c
FeCO3 MP
Discharge-2 V
Discharge-1.6 V
Discharge-1 V
Discharge-0.1 V
Incremental phase angle (°)
Frequency (Hz)
d
FeCO3 MP
Charge-0.1 V
Charge-0.8 V
Charge-1.4 V
Charge-1.8 V
Charge-2.4 V
Charge-3 V
Incremental phase angle (°)
Frequency (Hz)

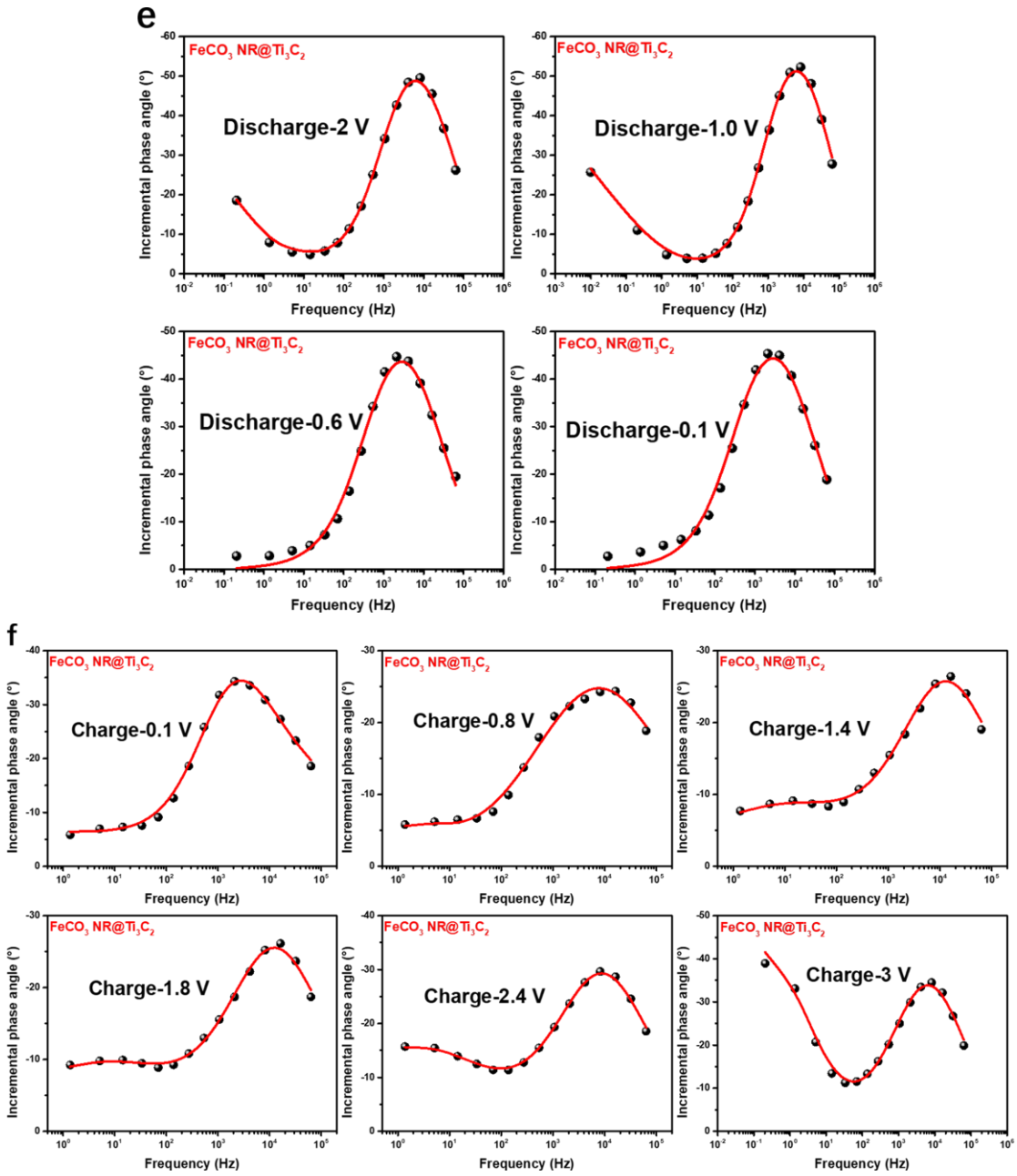

Figure S11. Equivalent circuits used to simulate different EIS spectra with (a) one semicircle and (b) two semicircles in Nyquist plots, respectively, as presented in Figure 4a and 4b. Where, the R_s stands for the cell resistance in the electrolyte, R_{ct} for the charge transfer resistance and R_f for the resistance of solid electrode interface film formed at the surface of active anode material. The CPE, CPE_1 and CPE_2 are constant phase elements, which are related to capacitive behaviors of electrons at different interfaces, and the W1 is Warburg impedance, which is associated with Li^+ diffusion within active anode material. Selected Bold plots at representative voltage states through fitting treatments of recorded EIS spectra during discharge and charge of (c, d) $FeCO_3$ MP and (e, f) $FeCO_3$ NR@Ti_3C_2 anode materials, respectively. The fitting of EIS spectrum was performed using the Zview software.

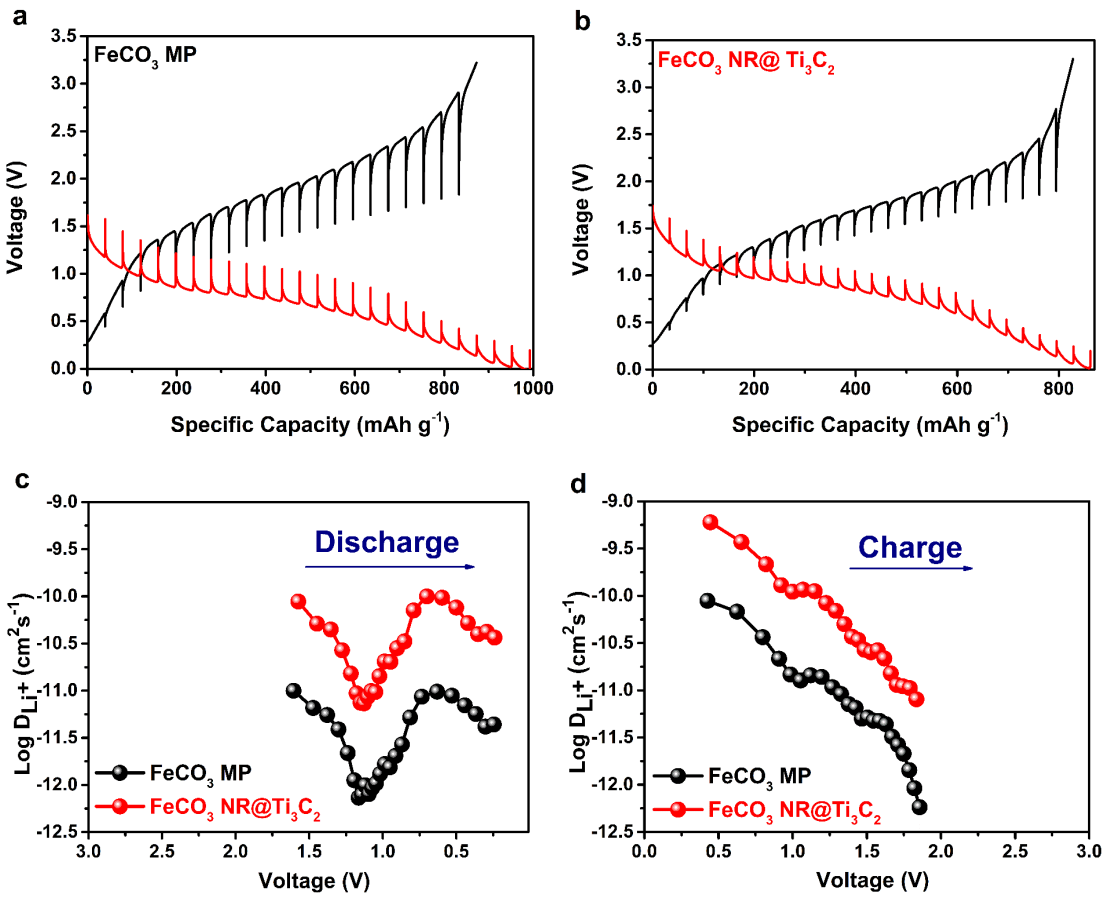

Figure S12. GITT curves of (a) $FeCO_3$ MP and (b) $FeCO_3$ NR@Ti_3C_2 anodes, together with corresponding calculated lithium ion diffusion coefficients (D_{Li}+) during (c) initial discharge and (d) initial charge as a function of voltages, respectively.

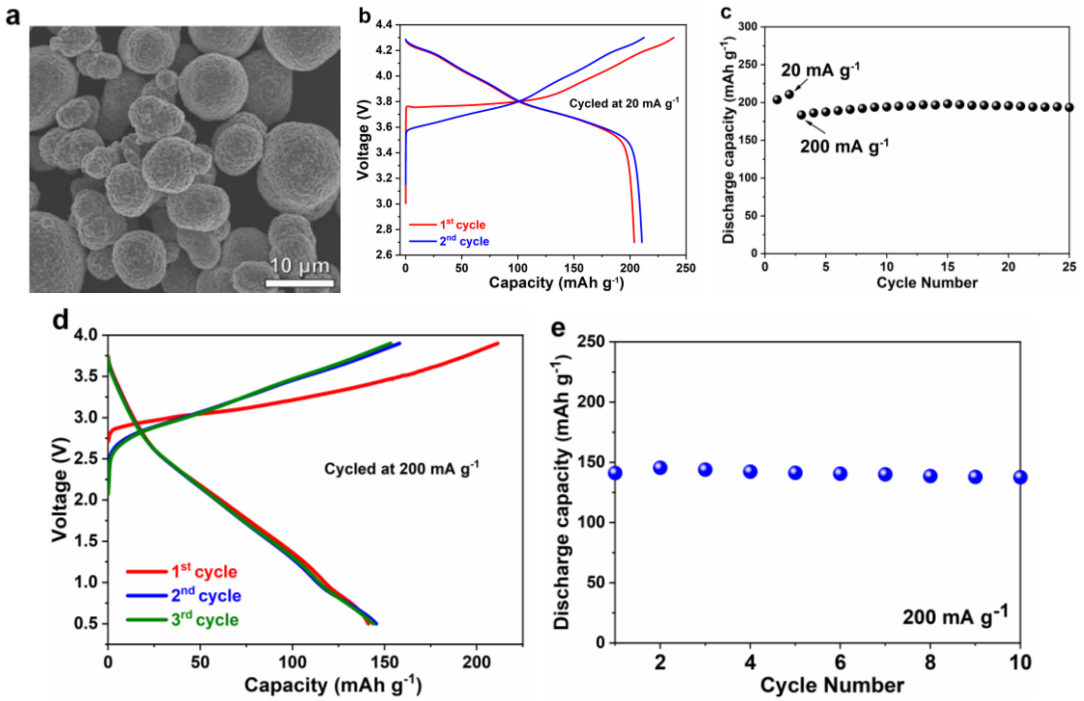

Figure S13. (a) SEM image, (b) charge/discharge curves in the first two cycles at 20 mA g^{-1} in a voltage range of 2.7-4.3 V *vs.* Li^+/Li and (c) cycling performance at 200 mA g^{-1} after two cycles at 20 mA g^{-1} of commercial NCM811 cathode material (RonBay Technology, Ningbo, China), and (d) charge/discharge curves in the first three cycles and (e) corresponding cycling performance of the full $FeCO_3$ NR@Ti_3C_2//NCM811 cell at 20 mA g^{-1} in a voltage range of 0.5-3.9 V.

Table S1. Capacity retention of the $FeCO_3$ NR@Ti_3C_2 anode at different current densities for prolonged cycles obtained in this work compared with various $FeCO_3$-and Fe_xO_y-based anode materials as reported in the literature.

Anode materials	Current density (mA g^{-1})	Cycle number	Specific capacity (mAh g^{-1})	References
$FeCO_3$ NR@Ti_3C_2	200	50	893	
$FeCO_3$ NR@Ti_3C_2	1000	500	529	This work
$FeCO_3$ NR@Ti_3C_2	2000	1000	280	
$FeCO_3$ (Cubes)	200	120	761	Ref. S3
$FeCO_3$ (MP)	200	200	710	Ref. S4
$FeCO_3$@graphene	200	40	883.7	Ref. S5
$FeCO_3$@CNT	200	140	694	Ref. S6
$FeCO_3$(nanorods)@RGO	200	80	789	Ref. S7
Fe_3O_4@Ti_3C_2	2500	800	278	Ref. S8
Fe_2O_3@Ti_3C_2-N	2000	400	549	Ref. S9
α-Fe_2O_3@Fe_3O_4	500	200	711	Ref. S10

Table S2. Lithium storage capacities delivered by the $FeCO_3$ NR@Ti_3C_2 anode at different current densities in this work compared with various $FeCO_3$- and Fe_xO_y-based anode materials as reported in the literature.

Anode materials	**(Current density) (A g^{-1})**	**0.1 (0.125)**	**0.2 (0.25)**	**0.4 (0.5)**	**0.8**	**1-3**	**References**
$FeCO_3$ NR@Ti_3C_2	Specific capacity (mAh g^{-1})	954	893	738 (0.5)		570 (1) 462 (2) 352 (3)	This work
$FeCO_3$@CNT			694	550	380	210 (1.2) 105 (3.2)	Ref. S6
$FeCO_3$(nano)@GO			789	699	500	260 (1.2)	Ref. S7
$FeCO_3$@graphene			842	675	559	358 (1)	Ref. S5
$FeCO_3$ MP		810	710	670	405	385 (1)	Ref. S4
$FeCO_3$(cubes)			761	725	595	430 (1.2)	Ref. S3
Fe_3O_4@Ti_3C_2		500 (0.125)	390 (0.25)	310 (0.5)		278 (1.25) 190 (2.5)	Ref. S8

Table S3. Extracted values of different parameters through fitting recorded EIS spectra during discharge and charge processes of the $FeCO_3$ MP anode material as shown in Figure 4a based on different equivalent circuits as presented in Figure S11a and S11b.

$FeCO_3$ MP Discharge/ Voltage states (V)	**R_s (Ω)**	**R_f (Ω)**	**CPE_1-T ($Ω^{-1}$ cm^{-2} S^{-n})**	**CPE_1-P ($Ω^{-1}$ cm^{-2} S^{-n})**	**R_{ct} (Ω)**	**CPE_2-T ($Ω^{-1}$ cm^{-2} S^{-n})**	**CPE_2-P($Ω^{-1}$ cm^{-2} S^{-n})**	**W_0 (Ω)**
2.0 V	3.95	--	--	--	107	6.9×10^{-6}	0.81	2.5
1.8 V	4.86	--	--	--	111	6.6×10^{-6}	0.81	28.1
1.6 V	4.32	--	--	--	116	5.7×10^{-6}	0.82	10.7
1.4 V	4.06	--	--	--	122	4.6×10^{-6}	0.83	17.1
1.2 V	3.95	--	--	--	133	4.4×10^{-6}	0.84	14.1
1.0 V	4.31	--	--	--	192	4.6×10^{-6}	0.82	824.7
0.8 V	4.08	--	--	--	168	5.0×10^{-6}	0.82	122
0.6 V	4.43	--	--	--	166	6.7×10^{-6}	0.80	62.5
0.4 V	4.35	--	--	--	168	7.3×10^{-6}	0.79	57.3
0.2 V	4.36	--	--	--	170	7.9×10^{-6}	0.78	55.2
0.1 V	4.43	--	--	--	176	8.4×10^{-6}	0.78	53.4
$FeCO_3$ MP Charge/ Voltage states (V)	**R_s (Ω)**	**R_f (Ω)**	**CPE_1-T ($Ω^{-1}$ cm^{-2} S^{-n})**	**CPE_1-P ($Ω^{-1}$ cm^{-2} S^{-n})**	**R_{ct} (Ω)**	**CPE_2-T ($Ω^{-1}$ cm^{-2} S^{-n})**	**CPE_2-P($Ω^{-1}$ cm^{-2} S^{-n})**	**W_0 (Ω)**
0.1 V	3.7	118	9.2×10^{-6}	0.81	107	0.016	2.66	125.8
0.2 V	5.1	78	3.2×10^{-5}	0.69	90.8	0.008	0.294	108.1
0.4 V	4.9	66	6.8×10^{-5}	0.64	80.34	0.012	0.372	533.2
0.6 V	4.7	46	1.5×10^{-4}	0.57	68.56	0.009	0.342	212.5
0.8 V	3.7	51	4.2×10^{-5}	0.73	78.42	0.023	0.209	69.8
1.0 V	4.1	30	3.5×10^{-5}	0.75	110.31	0.016	0.238	77.2
1.2 V	5.0	34	3.2×10^{-5}	0.76	98	0.012	0.291	92.7
1.4 V	6.0	44	4.7×10^{-5}	0.70	66	0.006	0.555	128.7
1.6 V	5.8	51	4.8×10^{-5}	0.71	95	0.006	0.548	177.4
1.8 V	5.7	56	5.0×10^{-5}	0.71	112	0.005	0.541	218.7
2.0 V	5.8	57	5.6×10^{-5}	0.70	118	0.004	0.573	265.5
2.2 V	5.7	60	5.9×10^{-5}	0.70	128	0.003	0.599	308.7
2.4 V	5.8	65	6.3×10^{-5}	0.69	138	0.003	0.637	394.6
2.6 V	5.9	106	6.6×10^{-5}	0.68	161	0.002	0.662	554.7
2.8 V	5.6	115	6.2×10^{-5}	0.68	472	0.002	0.675	712.8
3.0 V	5.8	158	6.0×10^{-5}	0.68	984	0.002	0.686	974.6

Table S4. Extracted values of different parameters through fitting recorded EIS spectra during discharge and charge processes of the $FeCO_3$ NR@Ti_3C_2 anode material as shown in Figure 4a based on different equivalent circuits as presented in Figure S11a and S11b.

$FeCO_3$ NR@Ti_3C_2 Discharge/ Voltage states (V)	**R_s (Ω)**	**R_f (Ω)**	**CPE_1-T ($Ω^{-1}$ cm^{-2} S^{-n})**	**CPE_1-P ($Ω^{-1}$ cm^{-2} S^{-n})**	**R_{ct} (Ω)**	**CPE_2-T ($Ω^{-1}$ cm^{-2} S^{-n})**	**CPE_2-P($Ω^{-1}$ cm^{-2} S^{-n})**	**W_0 (Ω)**
2.0 V	7.42	--	--	--	103	7.6×10^{-6}	0.78	1909
1.8 V	6.90	--	--	--	108	7.0×10^{-6}	0.79	1524
1.6 V	6.96	--	--	--	112	6.7×10^{-6}	0.79	1314
1.4 V	7.10	--	--	--	115	6.3×10^{-6}	0.80	1238
1.2 V	7.01	--	--	--	122	6.0×10^{-6}	0.80	827
1.0 V	7.11	--	--	--	168	5.7×10^{-6}	0.81	940
0.8 V	6.02	--	--	--	142	3.0×10^{-5}	0.74	39.1
0.6 V	5.94	--	--	--	135	3.1×10^{-5}	0.74	42.9
0.4 V	5.96	--	--	--	128	2.9×10^{-5}	0.74	46.8
0.2 V	5.86	--	--	--	132	2.9×10^{-5}	0.74	40.1
0.1 V	5.61	--	--	--	143	3.3×10^{-5}	0.73	66.4
$FeCO_3$ NR@Ti_3C_2 Charge/ Voltage states (V)	**R_s (Ω)**	**R_f (Ω)**	**CPE_1-T ($Ω^{-1}$ cm^{-2} S^{-n})**	**CPE_1-P ($Ω^{-1}$ cm^{-2} S^{-n})**	**R_{ct} (Ω)**	**CPE_2-T ($Ω^{-1}$ cm^{-2} S^{-n})**	**CPE_2-P($Ω^{-1}$ cm^{-2} S^{-n})**	**W_0 (Ω)**
0.1 V	5.88	96	2.8×10^{-5}	0.74	48.2	0.001	0.190	78.8
0.2 V	1.53	42	3.0×10^{-5}	0.81	37.3	0.014	0.195	74.1
0.4 V	5.29	46	1.5×10^{-4}	0.59	35.7	0.008	0.177	51.9
0.6 V	0.21	43	3.7×10^{-4}	0.50	26.5	0.012	0.077	43.7
0.8 V	4.37	36	2.8×10^{-4}	0.53	10.3	0.015	0.812	53.4
1.0 V	4.67	18	5.2×10^{-5}	0.68	36.2	0.010	0.386	54.4
1.2 V	4.70	18	5.5×10^{-5}	0.68	44.6	0.01	0.387	47.6
1.4 V	4.85	18	5.3×10^{-5}	0.69	50.1	0.008	0.415	74.4
1.6 V	4.94	20	4.8×10^{-5}	0.70	54.3	0.007	0.440	80.7
1.8 V	4.90	22	4.9×10^{-5}	0.69	64.1	0.006	0.468	93.8
2.0 V	4.97	24	4.3×10^{-5}	0.71	93.9	0.006	0.460	23.5
2.2 V	4.95	25	4.4×10^{-5}	0.70	141.2	0.006	0.476	34.2
2.4 V	4.96	25	4.6×10^{-5}	0.72	198.6	0.005	0.462	46.6
2.6 V	4.91	26	4.5×10^{-5}	0.72	221.5	0.007	0.441	128.5
2.8 V	4.94	27	4.2×10^{-5}	0.71	373.7	0.006	0.446	432.6
3.0 V	4.93	37	5.4×10^{-5}	0.68	792.2	0.005	0.578	879.5

References

1 X. Zhang, R. Lv, A. Wang, W. Guo, X. Liu, J. Luo, *Angew.Chem.*, 2018, **57**, 15028-15033.

2 Hu, J. Wang, H. Zhang, Z. Li, M. Hu, X. Wang, *Phys. Chem. Chem. Phys.*, 2015, **17**, 9997-10003

3 C. Zhang, W. Liu, D. Chen, J. Huang, X. Yu, X. Huang, Y. Fang, *Electrochim. Acta*, 2015, **182**, 559-564.

4 Y. Zhong, L. Su, M. Yang, J. Wei, Z. Zhou, *ACS Appl. Mater. Interfaces*, 2013, **5**, 11212-11217.

5 B. Yao, Z. Ding, X. Feng, L. Yin, Q. Shen, Y. Shi, J. Zhang, *Electrochim. Acta*, 2014, **148**, 283-290.

6 F. Li, W. Liu, K. Li, W. Chen, D. Xu, X. Yu, H. Hu, *J. Electroanal. Chem.*, 2018, **824**, 67-74.

7 D. Xu, W. Liu, C. Zhang, X. Cai, W. Chen, Y. Fang, X. Yu, *J. Power Sources*, 2017, **364**, 359-366.

8 Y. Wang, Y. Li, Z. Qiu, X. Wu, P. Zhou, T. Zhou, J. Zhao, Z. Miao, J. Zhou, S. Zhuo, *J. Mater. Chem. A*, 2018, **6**, 11189-11197.

9 Z. Zhang, L. Weng, Q. Rao, S. Yang, J. Hu, J. Cai, Y. Min, *J. Power Sources*, 2019, **439**, 227107.

10 H. Liu, S. Luo, D. Hu, X. Liu, Q. Wang, Z. Wang, Y. Wang, L. Chang, Y. Liu, T. Yi, Y. Zhang, A. Hao, *Appl. Surf. Sci*, 2019, **495**, 143590.